Acta Metallurgica Sinica (English Letters)
https://doi.org/10.1007/s40195-020-01116-x

Detoxication and Theranostic Aspects of Biosynthesised Zinc Oxide Nanoparticles for Drug Delivery

Krishnaswamy Kanagamani[1] · Pitchaipillai Muthukrishnan[2] · Ayyasami Kathiresan[2] · Karikalan Shankar[2] · Pandurengan Sakthivel[3] · Murugan Ilayaraja[4]

Received: 3 June 2020 / Revised: 28 June 2020 / Accepted: 8 July 2020

Abstract
Bioactive materials obtained from plant bio-resources offer immense attention for development and production of nanotechnology enabled products for biomedical applications. In the present study, *Ficus hispida* leaf extract (FHLE) was used as a stabilising agent for the environmentally benign synthesis of zinc oxide nanoparticles (ZnO-NPs) which were investigated for prospective versatile applications (anticancer and photocatalytic activities). The formation of ZnO-NPs was confirmed by UV–visible spectra. Wurtzite (hexagonal) form of the herb-assisted synthesised ZnO-NPs with particle size ranging from 20 to 200 nm was confirmed by transmission electron microscopy (TEM) analysis. In vitro analysis was carried out against Dalton's lymphoma ascites (DLA) cell lines by trypan blue assay, the results revealed 96% inhibition at concentration of 200 μg ml^{-1}, and the photodegradation experiments carried out for degradation of Congo red revealed complete degradation of the dye after 70 min of exposure to UV light.

Keywords Zinc oxide nanoparticles · Anticancer activity · Photocatalysis · Congo red

1 Introduction

Nanoparticle synthesis has attracted much attention in recent years. Nanoparticles possess atom-like properties due to the large surface area, high surface energy, a high fraction of surface atoms, and increased energy gap in their atomic size [1–3]. The interesting properties of the nanoparticles pave way for research on novel methods for synthesis. Among various metal oxide nanoparticles, ZnO-NPs attract tremendous attention because of its unique property of high excitation binding energy of 60 meV and band gap of 3.3 eV [4–6]. Nanomaterials can be synthesised through various physical and chemical methods which include pulsed layer deposition [7], thermal deposition [8], chemical microemulsion [9], wet chemical [10], spray pyrolysis, electro-deposition, etc. Nowadays, metal oxide nanoparticles are synthesised by physical and chemical methods which include expensive usage of hazardous reagent, toxic organic solvents, and high pressure. The environmental and biological risk associated with traditional physical and chemical methods limits the usage of medical applications. Therefore, there is a challenge for the development of simple, eco-friendly, rapid, and energy efficient process for the synthesis of nanoparticles with catalytic behaviour. Hence, in spite of physical and chemical protocols, environmentally safe synthesis of nanoparticles has received considerable attention in recent years and various available plant bio-resources have been efficiently studied for the synthesis of nanoparticles as reported in the literature [11–17]. The green method, using plant bio-resource, is a simple and alternative to physical and chemical methods without the use of any toxic and expensive chemicals. *Ficus hispida*, a traditional medicinal plant belonging to the family of Moraceae, was found to possess bioactive groups required for the formation and

Available online at http://link.springer.com/journal/40195.

✉ Pitchaipillai Muthukrishnan
mukepmk@gmail.com

[1] Department of Chemistry, SNS College of Technology, Coimbatore 641035, India

[2] Department of Chemistry, Faculty of Engineering, Karpagam Academy of Higher Education, Coimbatore 641021, India

[3] Department of Physics, Faculty of Engineering, Karpagam Academy of Higher Education, Coimbatore 641021, India

[4] Department of Chemistry, Arumugam Pillai Seethai Ammal College, Tirupattur 630211, India

Published online: 14 August 2020

stabilisation of nanoparticles. In spite of these bioactive groups in *Ficus hispida* leaf extract, it is used as a reducing agent for the biosynthesis of Ag-NPs [18]. Various applications of nanoparticles have been explored in the reported literature, such as antioxidant [19], antidiabetic [20], antifungal [21], antibacterial [19, 22], anticancer [23, 24], and photocatalytic performance. [25–29].

Due to the remarkable characteristics of zinc oxide nanoparticles, they are extensively engaged in several practical applications. Compared to other super capacitor materials, i.e. TiO_2, SiO_2 and SnO_2 which have wide band gap energy, ZnO shows enhanced photocatalytic properties. ZnO doped with various metal ions has been reported for the photocatalytic degradation of dyes such as Acid Black 210 [30], Acid Black 234 [31, 32], and organic compounds [33]. Metal oxide nanoparticles doped with d-block elements like Mn, Fe, Sn, Co are used as anticancer [34], antioxidant [36, 37], antibacterial [38], optical [39], and also as photocatalyst [35].

Environmental problems associated with the discharge of dye effluents into water lead to active research in the field of environmental management. Dye removal from waste water is one of the important tasks to be faced. Among the various dye contaminants, Congo red is an important azo dye, which is also used as a staining agent in textile industry. These dyes are hazardous to human health and aquatic life when discharged into water. Conventional dye removal process from waste water includes chemical coagulation/flocculation, oxidation [40], biodegradation, adsorption, etc. [41, 42], with several disadvantages associated with the various reported processes. There is a need to develop novel methods using cost-effective semiconductor nanoparticles as catalyst. Among the semiconductor nanoparticles, ZnO-NPs are reported to possess photodegradation properties against various pollutants like phenol [43] and methyl orange [44, 45]. In this work, ZnO-NPs were synthesised and characterised using *Ficus hispida* leaf extract as bio-reductant for the first time, and synthesised ZnO-NPs were found to have anticancer activity and also photocatalytic activity for degradation of Congo red dye.

2 Experimental

2.1 Preparation of *Ficus hispida* leaf extract (FHLE)

Ficus hispida leaves, collected from Karpagam institution campus in Coimbatore, were washed well with deionised water to remove grime particles and then were chopped into small pieces. The 50-g freshly chopped leaves were boiled with 500 ml deionised water at 90℃ for 5 min. The obtained pale yellow solution was cooled in a well-ventilated area (approximately 28 ℃), filtered through Whatman filter, and refrigerated for further use.

2.2 Environmentally beneficent synthesis of zinc oxide nanoparticles

The zinc nitrate used in the synthesis was of analytical grade (99.9%) and obtained from S.D. Fine chemicals. The schematic representation of biosynthesis of *Ficus*-mediated ZnO-NPs is given in Fig. 1. 20 ml of FHLE was added to 80 ml of zinc nitrate in the reaction vessel and stirred using a magnetic stirrer at ambient temperature for 4 h. The pale yellow solution thus obtained was dried at 100 °C in an oven. The resultant mass was subjected to calcination at 400 °C to obtain fine crystals of ZnO-NPs and stored for further characterisation.

2.3 Potential Mechanism for the Formation of Zinc Oxide Nanoparticle

The GC–MS analysis of *Ficus hispida* leaf extract [18] showed stigmasterol (peak area 82.38%) as the major component. Other remarkable components included neophytadiene (1.35%), 5-(hydroxymethyl)-2-furancarbox aldehyde (0.14%), 2-(benzyloxymethyl)-5-methylfuran (0.06%), palmitic acid (1.16%), sitosterols (2.91%), phytol (1.43%), ethyl linoleate (0.34%), and 2,3-dihydro-3,5-dihydroxy-6-methyl-pyran-4-one (0.12%). Figure 2 depicts the mechanism for the formation of ZnO-NPs. Stigmasterol, a phytosterol with the molecular formula ($C_{29}H_{48}O$), plays a vital role in the formation of ZnO-NPs. The stigmasterol present in the leaf extract combined with zinc nitrate to form a weak complex, i.e. zinc–stigmasterol complex via weak hydrogen bonds. This complex solution was then dried in a hot air oven for 8 h, and hydroxide complex was thus obtained. The hydroxide complex undergoes calcination to form ZnO-NPs. Among the phytocompounds found in *Ficus hispida* leaf extracts, stigmasterol easily attracts metals due to its phenolic content. It was also present as a major constituent. Reported results showed that it is difficult to interpret the formation mechanism of nanoparticle. In this work, the possible mechanism that drives the synthesis of ZnO-NPs was reported.

2.4 Characterisation of *Ficus*-Mediated ZnO-NPs

The optical properties of biosynthesised ZnO-NPs were evaluated using double-beam UV-1601 Shimadzu spectrophotometer in the range of 290–450 nm. FT-IR spectra were recorded for the eco-friendly synthesised ZnO-NPs at room temperature using BRUKER FTIR-TENSOR-27 spectrophotometer instrument in order to analyse and detect functional

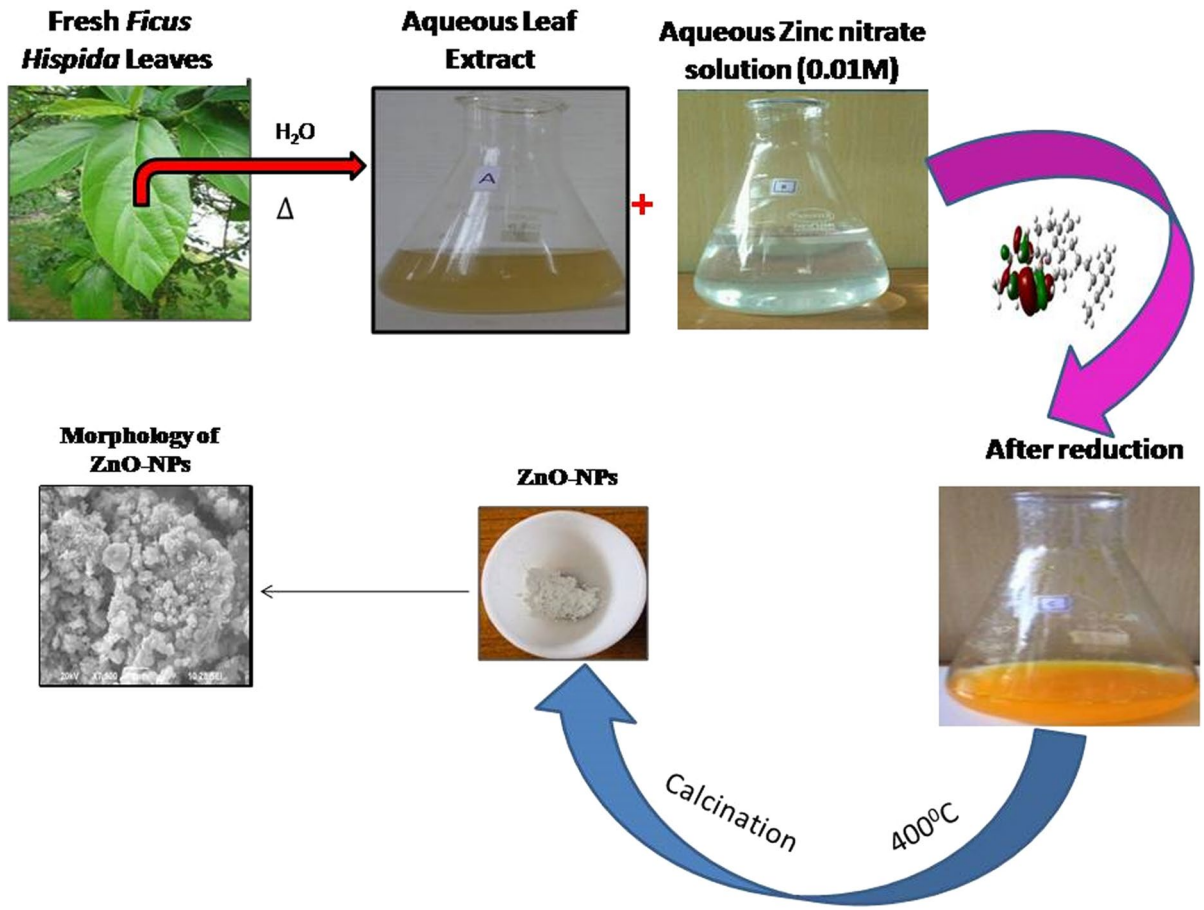

Fig. 1 Schematic illustration of synthesis process of zinc oxide nanoparticles

groups. The size and surface morphology of ZnO-NPs were observed by scanning electron microscopy (SEM) (JEOL JSM 6390). The element composition of synthesised ZnO-NPs was analysed by energy-dispersive X-ray spectroscopy (EDX). The synthesised ZnO-NPs were characterised by high-resolution transmission electron microscopy (HR-TEM) (JEOL JEM 2100). The size of ZnO-NPs in HR-TEM was measured by using the Image J software. The crystalline nature of ZnO-NPs was analysed by X-ray diffraction analysis (XRD) (SHIMADO-Model XRD 6000). The scanning was carried out between 20° and 90° at a scanning rate of 0.05° min^{-1}, and the time constant is 2 s.

2.5 In vitro Cytotoxicity Assay

As-prepared ZnO-NPs were tested for anticancer activity against Dalton's lymphoma ascites (DLA) cells (The in vitro cytotoxicity tests were carried out in Amala Cancer Research Institute, Kerala.) The assay was performed using trypan blue exclusion method. The tumour cells were obtained from intraperitoneal cavity of tumour bearing mice using a sterile disposable syringe and were suspended in phosphate-buffered saline (PBS) or normal saline. After adjusting the cell density to concentration (1×10^6 cells in 0.1 mL), it was suspended with different concentrations of ZnO-NPs ranging from 10–200 μg mL^{-1} and then, the volume of the tubes was adjusted up to 1 mL using PBS along with the control tumour cell suspension. The assay mixture was incubated at 37 °C for 3 h. Cell viability was assessed by adding 0.1 mL of 1% trypan blue dye solution using haemocytometer, and viable and non-viable cells were counted. Cytotoxicity can be calculated according to Eq. (1):

$$\text{Cytotoxicity} = \frac{\text{Number of dead cells}}{\text{Number of live cells} + \text{Number of dead cells}} \times 100\%. \quad (1)$$

2.6 Photocatalytic Degradation Studies of *Ficus*-Mediated ZnO-NPs

The photocatalytic activity of ZnO-NPs was performed and assessed by evaluating the degradation of Congo red

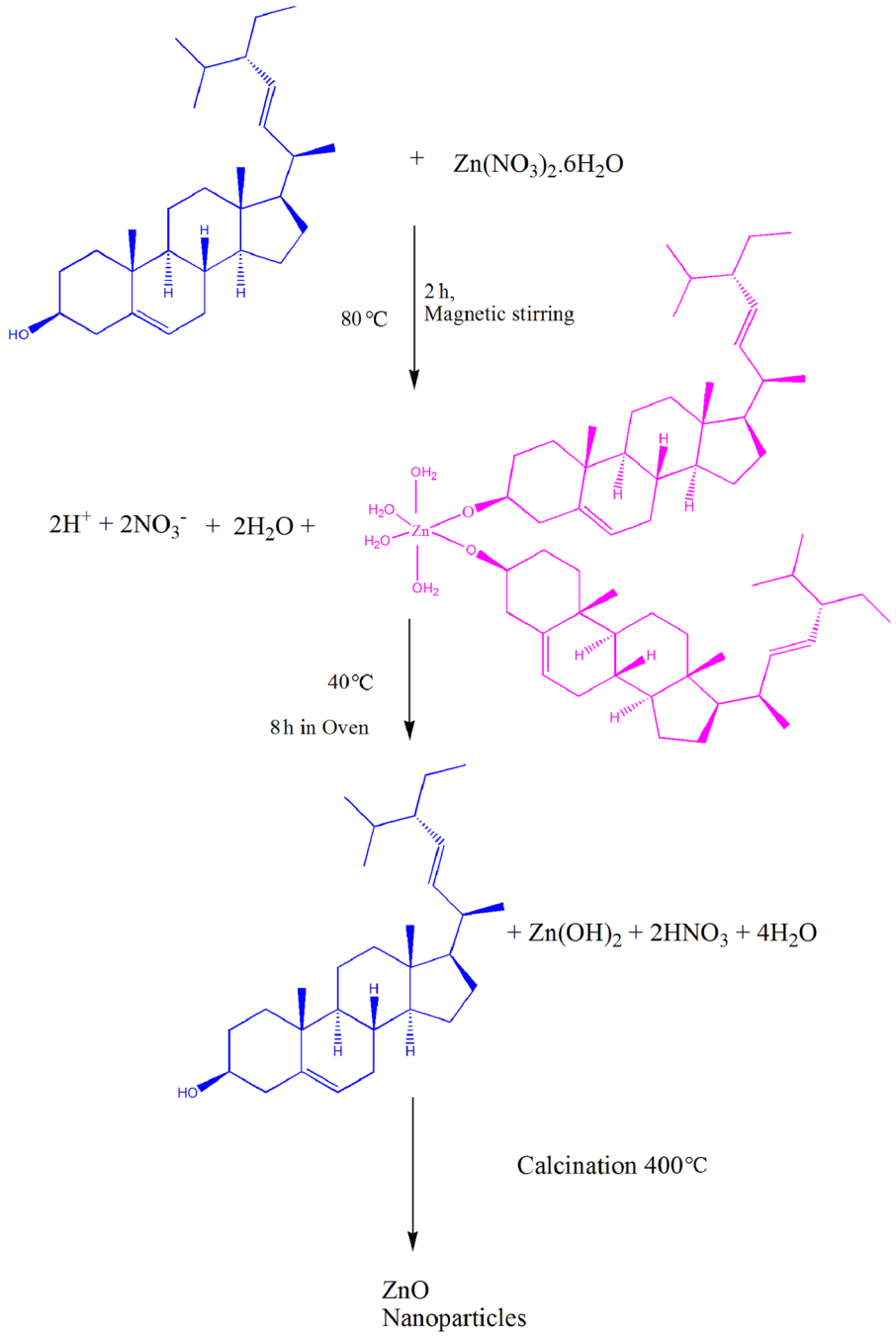

Fig. 2 Possible formation mechanism for zinc oxide nanoparticle

under UV irradiation. 50 mg of the green catalyst (ZnO-NPs) was added with 75 mL of (10 mg L^{-1}) of anionic dye (Congo red) solution in 100-ml beaker. The reaction mass was stirred in a magnetic stirrer for about 1 h in dark condition. Then, the reaction vessel was kept under UV light irradiation for different time intervals. The progress of degradation process was analysed using UV–visible spectrophotometer. The degradation rate of Congo red solution was estimated using Eq. (2):

$$\text{Degradation rate} = (I_0 - I)/I_0 \times 100\%, \quad (2)$$

where I is the absorption peak intensity of Congo red at various time intervals and I_0 is the absorption intensity of the initial Congo red solution.

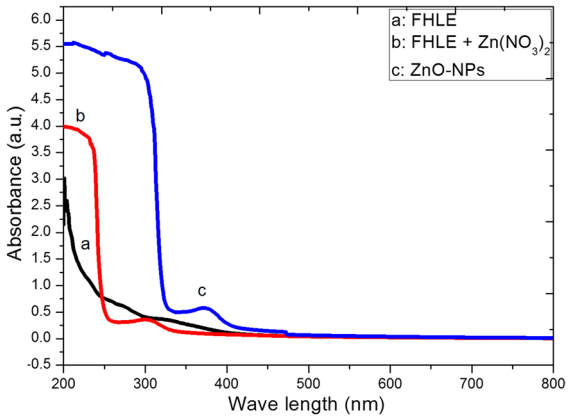

Fig. 3 UV–Visible spectra of *Ficus hispida* leaf extract, mixture of *Ficus hispida* leaf extract and zinc nitrate, and zinc oxide nanoparticles

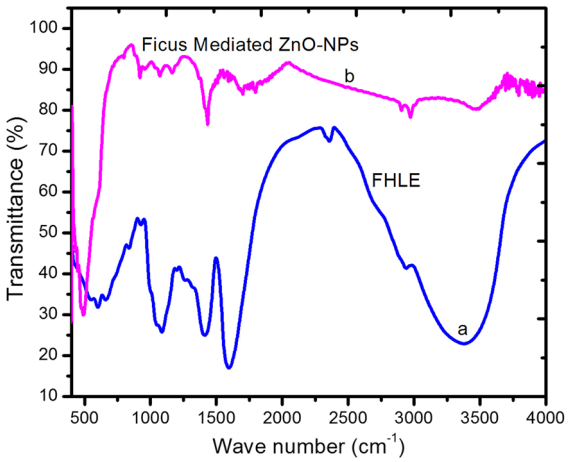

Fig. 4 FT-IR spectrum of *Ficus hispida* leaf extract and *Ficus*-mediated zinc oxide nanoparticles

3 Results and Discussion

3.1 Electronic Spectroscopic Analysis

The milestone properties of ZnO nanoparticles were characterised using UV–Vis spectroscopy. UV–Vis spectrum of the FHLE, *Ficus hispida*, and zinc nitrate, and biosynthesised ZnO-NPs is given in Fig. 3. The FHLE absorbance is at 204 nm, and the intermediate Zn $(OH)_2$ is found to have absorbed at 301 nm. It was reported that there was no absorption band for zinc nitrate solution [46]. From the spectrum (Fig. 3), it is confirmed that there is no absorbance peak of FHLE and zinc hydroxide in the spectrum of biosynthesised ZnO-NPs and hence reveals the purity of synthesised nanoparticles. The surface plasmon resonance (SPR) band at 376 nm confirms the formation of the zinc oxide nanoparticles. Surface plasmon resonance (SPR) is the resonant oscillation of conduction electrons at the interface between negative and positive permittivity material stimulated by incident light, and it is the characteristic of the obtained nanoparticles which agrees with the reported studies on the biosynthesis of ZnO-NPs (absorption peak at 374 nm) using different herbal extracts [47, 48], confirming the presence of ZnO nanoparticles.

3.2 Changes in Functional Groups by FT-IR Analysis

FT-IR spectra of FHLE and ZnO-NPs are given in Fig. 4. FT-IR spectra of the *Ficus hispida* having peaks at 3383 cm^{-1} and 2926 cm^{-1} indicate the presence of -OH and C-H stretching. The absorption peak at around 1625 cm^{-1} represents C = O stretching. The bands at 1402 cm^{-1} are associated with C–C stretching of an aromatic ring. The absorption peak at 1060 cm^{-1} is attributed to C–O–C stretching. FT-IR spectra of ZnO-NPs reveal a weak absorption at 2852 cm^{-1} and 2922 cm^{-1} which can be assigned to -C-H stretching of carboxylic acids and aliphatic asymmetric C-H stretching vibrations. The peak at 1745 cm^{-1} is due to C = O stretching vibrations of the carbonyl group. The weak absorption peaks at 1164 cm^{-1} and 1322 cm^{-1} are indicative of C = N stretching of amide bonds. The peaks at 744 cm^{-1} and 669 cm^{-1} correspond to R-CH group and stretching vibrations of ZnO which correlates with the reported data. The peak at 441 cm^{-1} is assigned to metal oxygen [Zn–O] bond as reported in the previous studies [49, 50].

3.3 Purity and Morphological Analysis of ZnO-NPs

The morphological and structural characterisation of the synthesised ZnO nanoparticles was investigated by SEM, as shown in Fig. 5a. It is evident from the result that the biosynthesised ZnO nanoparticles show agglomerations of ZnO-NPs. The agglomeration shows the presence of nanoparticle aggregates. The purity of the synthesised ZnO nanoparticles was confirmed by EDX analysis. The peaks corresponding to Zn and O were found, and no impurity peaks were detected (Fig. 5b). This clearly confirms that the synthesised nanoparticles are pure and consist only of pure Zn and O. The weight and atomic percentages of Zn and O are listed in Table. 1. The weight percentage of Zn and O is 81.35% and 18.65%, respectively, which indicates the synthesised ZnO nanoparticles comprising only of Zn and O without any impurities. The atomic percentage is approximately stoichiometric ratio of 1:1.

The HR-TEM micrograph of green synthesised ZnO-NPs (Fig. 6) reveals hexagonal (wurtzite) shape of ZnO-NPs with the particle size in the range of 10–200 nm which is in accordance with XRD data. In the literature [51], particle sizes of ZnO-NPs are in the range of 14–27 nm that supports the existing morphology of synthesised ZnO-NPs.

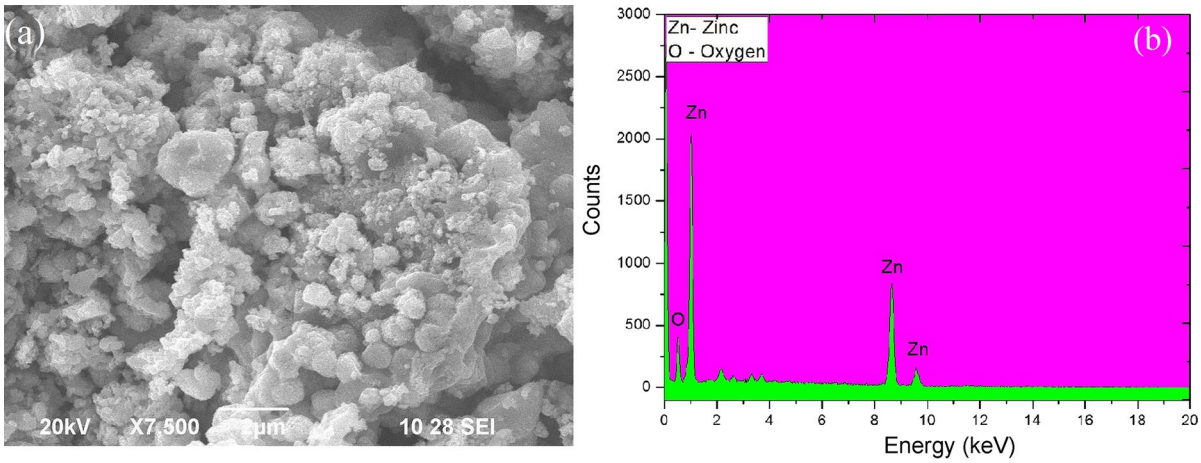

Fig. 5 Morphology and element analysis of zinc oxide nanoparticles: **a** SEM image, **b** EDX spectrum of pure zinc oxide nanoparticles

Table 1 Weight and atomic percentages of ZnO nanoparticles

Element	Wt.%	At.%
O	18.65	53
Zn	81.35	47

In the literature [52], it is found that the nanoparticle size is 30–40 nm and shows polyhedral in shape. The observed agglomeration of ZnO-NPs is due to high surface energy during its synthesis in aqueous medium. The selected area electron diffraction (SAED) pattern suggests that ZnO-NPs are crystalline and rings contain spots, indicating the polycrystalline nature.

3.4 XRD Analysis

The XRD analysis of the *Ficus*-mediated ZnO-NPs reveals the crystallographic structure of the synthesised nanoparticles. The obtained diffraction peaks at 32.01, 34.7, 37, 47.48, 56.9, 63.1, 66.2, 69.4 and 77.2 as given in Fig. 7 are attributed to Miller–Bravais lattices of [100], [002], [101], [102], [110], [103], [112], [201], and [202] planes, respectively. The obtained results agree with JCPDS file No. 036–1451 confirming the hexagonal wurtzite structure [53]. The product is found to have a fine crystalline structure as evidenced by the sharper and stronger diffraction peaks. No other additional peaks obtained suggest the purity of the synthesised ZnO-NPs.

3.5 In vitro Cytotoxicity Assay

The anticancer activity of bio-inspired nanoparticles against various cancer cell lines has been reported [54–57]. In vitro assay was done for as-prepared ZnO-NPs by trypan blue dye exclusion method against DLA cell lines. The results reveal that percentage inhibition of the DLA cells increases with increasing concentration of ZnO-NPs from 10 to 200 μg mL^{-1} as listed in Table 2. In this work, the maximum inhibition of cancer cells occurs at 200 μg mL^{-1} and it is observed that percentage of cell death increases with the increase in the concentration of ZnO-NPs. It is due to the intracellular release of dissolved zinc ions, followed by reactive oxygen species (ROS) induction. This may also be due to zinc-mediated protein activity disequilibrium and oxidative stress that eventually kill the cell. When ZnO-NPs nanoparticles are used as anticancer agent having a redox reaction system in them, they may react with the increased amount of chemical species signalling the molecules around them, producing even more ROS, resulting in huge oxidative stress in the cell and eventually killing the cancer cell [54]. In this study, it is found that prepared ZnO-NPs have comparable activity with standard drug (curcumin) as listed in Table 2 [58] and it is proved to have better antitherapeutic potential.

3.6 Photocatalytic Efficiency of ZnO-NPs

The photodegradation ability of the prepared ZnO-NPs was studied for Congo red dye under UV light and was explained with UV–Vis spectra, showing strong absorption at 490 nm with 50 mg of control dye as shown in Fig. 8A. The photocatalytic degradation was carried out by the prepared ZnO-NPs as catalyst and in the presence of UV light. The recorded UV spectrum reveals degradation of Congo red dye with decreasing absorption intensity and reaches almost zero after 70 min of exposure time.

The amount of catalyst loaded is an important parameter in degradation studies. The effects of dye degradation using various amounts of ZnO-NPs are shown in Fig. 8B. The results reveal that the percentage of degradation does not change when the amount of catalyst is

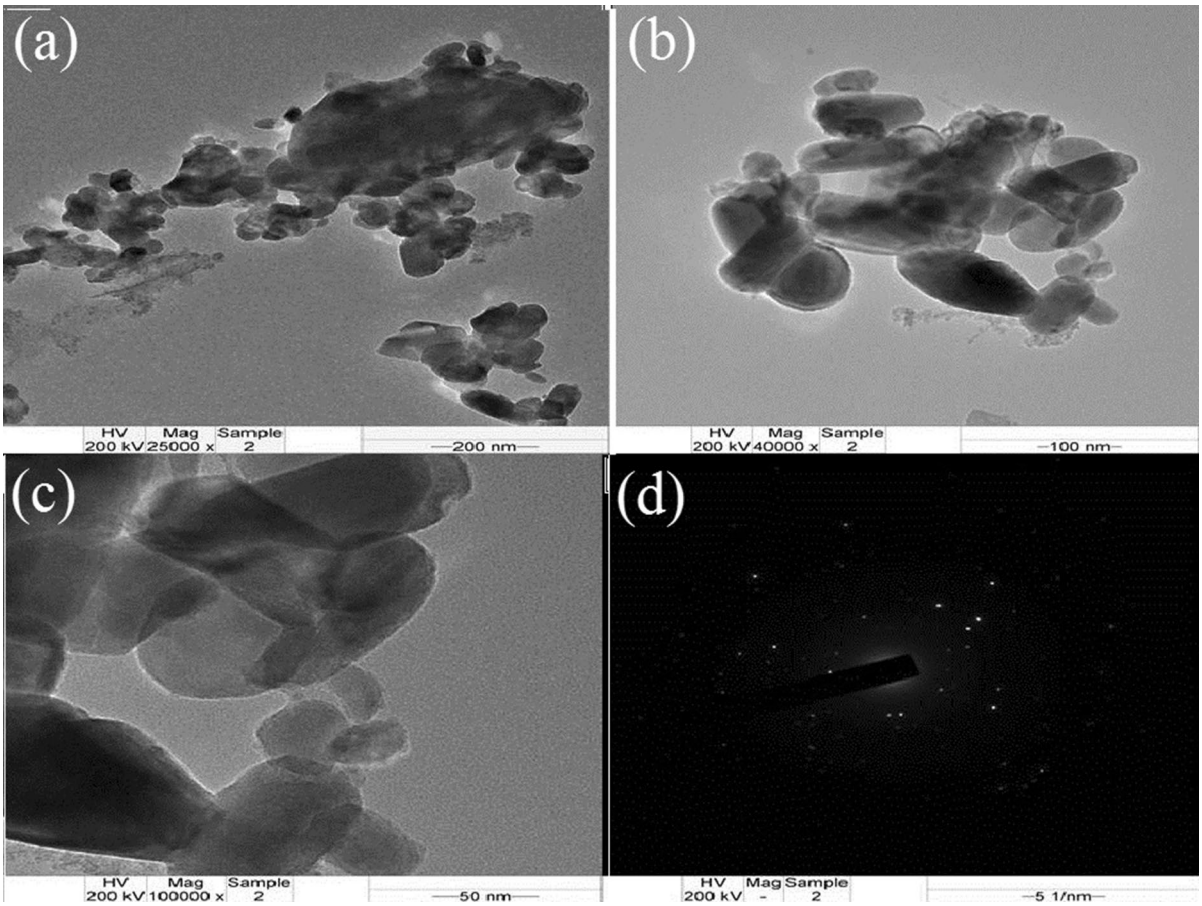

Fig. 6 TEM images of hexagonal shape of ZnO-NPs at different magnifications: **a** 200 nm, **b** 100 nm, **c** 50 nm, **d** the corresponding SAED pattern

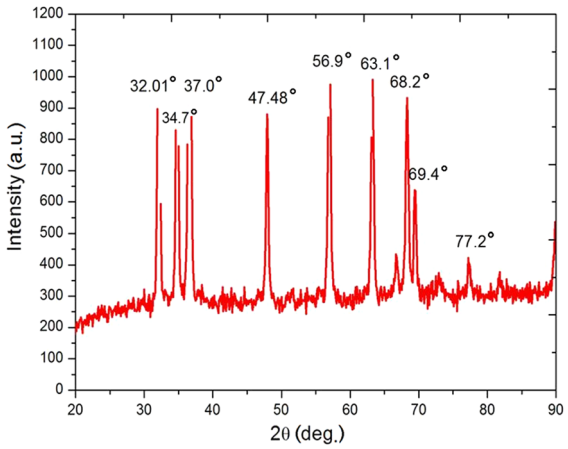

Fig. 7 XRD pattern of hexagonal wurtzite structure of ZnO-NPs

Table 2 Anticancer assay of *Ficus*-mediated ZnO-NPs on DLA cell lines

No	Concentration (µg mL^{-1})	Cell death (DLA) (%)	
		Ficus-mediated ZnO-NPs	Standard drug curcumin
1	10	19	41
2	20	36	54.47
3	50	57	69.71
4	100	77	81.69
5	200	96	100

increased beyond 50 mg. Figure 8C describes that no significant degradation is observed in the absence of catalyst and light. In addition, *Ficus*-mediated ZnO-NPs exhibit excellent degradation performance in the absence of light and catalyst. From the observations, it is confirmed that *Ficus*-mediated ZnO-NPs have excellent photocatalytic degradation performance. The analysis of optimum loading for efficient removal of dye avoids the excess usage of catalyst. The decolourisation efficiency increases from 45 to 98% as the catalyst dosage is increased from 20–70 mg. However, when the amount of the catalyst was further

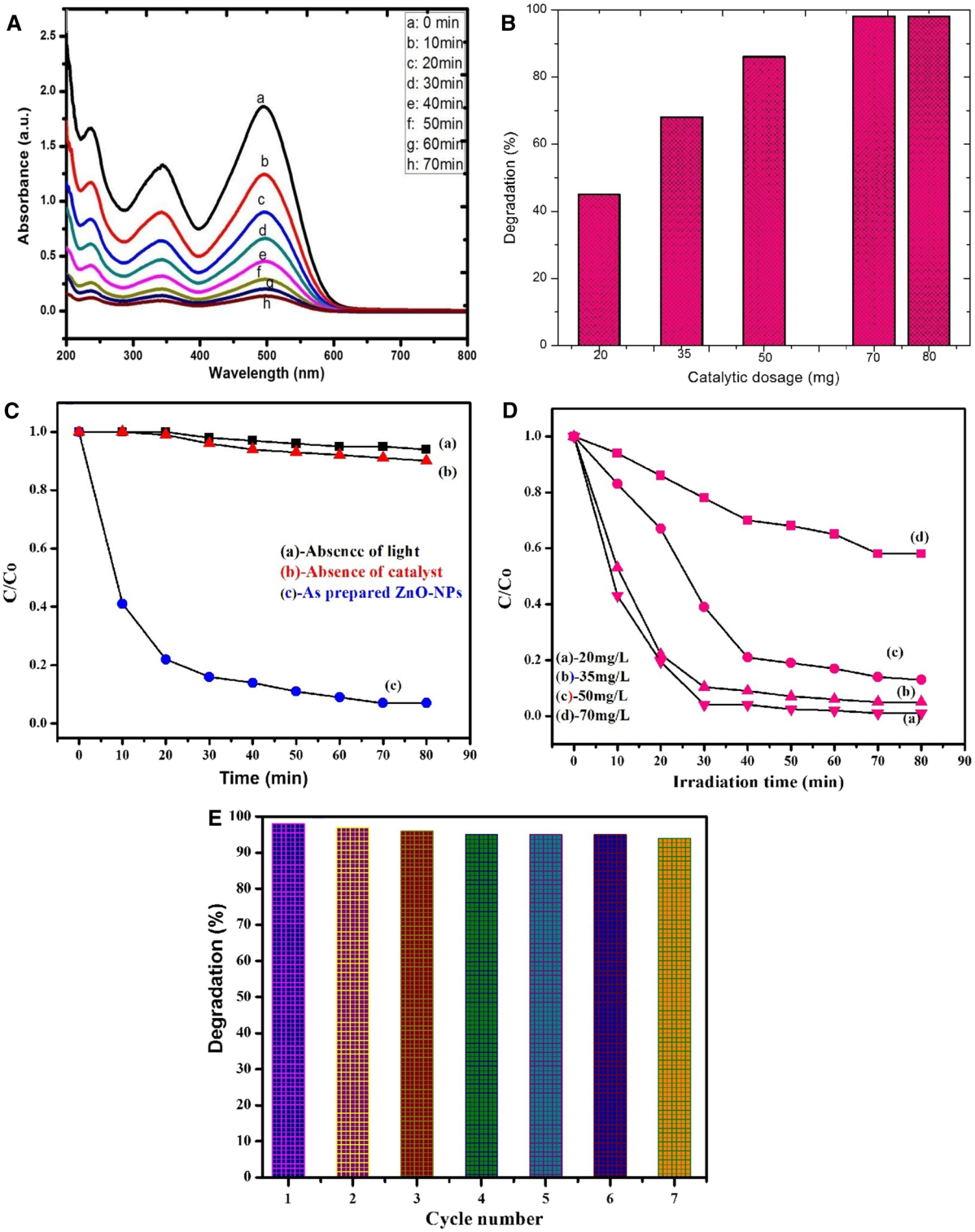

Fig. 8 UV spectrum of photodegradation of Congo red: **A** different time intervals, **B** effect of catalytic dosage, **C** comparison of photodegradation of Congo red, **D** effect of irradiation time with different loadings of catalyst and **E** recycle ability of ZnO-NPs

increased to 70 mg, the degradation rate did not change significantly as shown in Fig. 8D. The reusability and photostability of the prepared catalyst were analysed by conducting additional experiments in consecutive cycles for the photodegradation of Congo red under UV light irradiation, and the results are displayed in Fig. 8E. The

Table 3 Comparison of degradation ability of various biosynthesised ZnO-NPs and doped ZnO-NPs against various water pollutant

Source	Nanoparticle and size	Pollutant	Light source (UV/visible irradiation)	Percentage degradation (%)	Ref
Artocarpus heterophyllus leaf	ZnO-NPs & 10–15 nm	Congo red	UV irradiation	90	[59]
Carissa edulis fruit	ZnO-NPs & 50–55 nm	Congo red	UV–Vis irradiation	97	[60]
Sea buckthorn fruit	ZnO-NPs & 17.5 nm	Congo red	UV irradiation	99	[61]
Averrhoe carrambola fruit	ZnO-NPs & 20 nm	Congo red	UV irradiation	93	[62]
Avocado fruit peel	ZnO-NPs & 22–35 nm	Congo red	Solar irradiation	99	[63]
$ZnSO_4 \bullet 7H_2O$ and Ag_2SO_4	Ag/ZnO & 20–30 nm	Methyl violet (6B)	UV irradiation	93	[64]
$Zn(CH_3COO)_2$ $2H_2O$ + *Bamboo* charcoal + $AgNO_3$	ZnO-Ag/BC & 52 nm	Methylene blue	Visible irradiation	93.95	[65]
$Zn(CH_3COO)_2$ $2H_2O$ + *Bamboo* charcoal + $AgNO_3$	ZnO-Ag/BC & 52 nm	Malachite green	Visible irradiation	95.75	[65]
Ficus hispida leaf	ZnO-NPs & 20–200 nm	Congo red	UV irradiation	100	In the present study

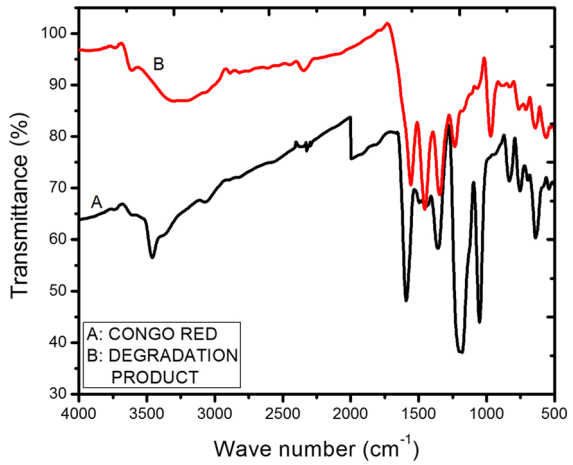

Fig. 9 FT-IR spectra of Congo red and degradation product

experiments show that *Ficus*-mediated ZnO-NPs have only negligible change in catalytic activity even after 7 days. The present study reveals that biosynthesised ZnO-NPs can be used as a photocatalyst for the degradation of organic dyes from waste water and play an important role in water treatment process compared to conventional methods. The degradability of biosynthesised ZnO-NPs is compared against the various reported synthesised ZnO-NPs as given in Table 3 [59–65].

3.6.1 Analysis of Degradation Product by FT-IR

The decolourisation mechanism of Congo red dye using biosynthesised ZnO nanoparticles as photocatalysts was analysed by FT-IR analysis. The Congo red dye and its degradation products were analysed by FT-IR analysis after decolourisation with photocatalyst. Figure 9 reveals the changes in the functional groups. The peak obtained at 1064 cm^{-1} in the Congo red spectrum is due to S = O stretching of the dye. The absorption peak at 3465 cm^{-1} represents the free N–H group of the dye. The N = N stretching of the azo group is obtained between 1584 and 1611 cm^{-1}. The FT-IR spectrum of degradation products reveals the changes in absorption peaks in comparison with spectrum of pure Congo red. The absorption peak at 511 cm^{-1} is due to aromatic ring bending vibration. The peaks at 703 cm^{-1} and 811 cm^{-1} are due to disubstitution aromatic ring vibrations. The peak at 1584 cm^{-1} is the characteristic of N = N stretching vibrations in the FT-IR spectrum of the degradation products obtained.

3.6.2 Degradation Route of Anionic Dye

Figure 10 represents the degradation pathway of Congo red using bio-inspired ZnO-NPs as photocatalysts. The possible degradation of the Congo red starts with the degradation into biphenyl-1–4′-diamine (m/z: 185, molecular weight:183) and the unidentified intermediate where the cleavage occurs at azo bond which is also supported by FT-IR measurements.

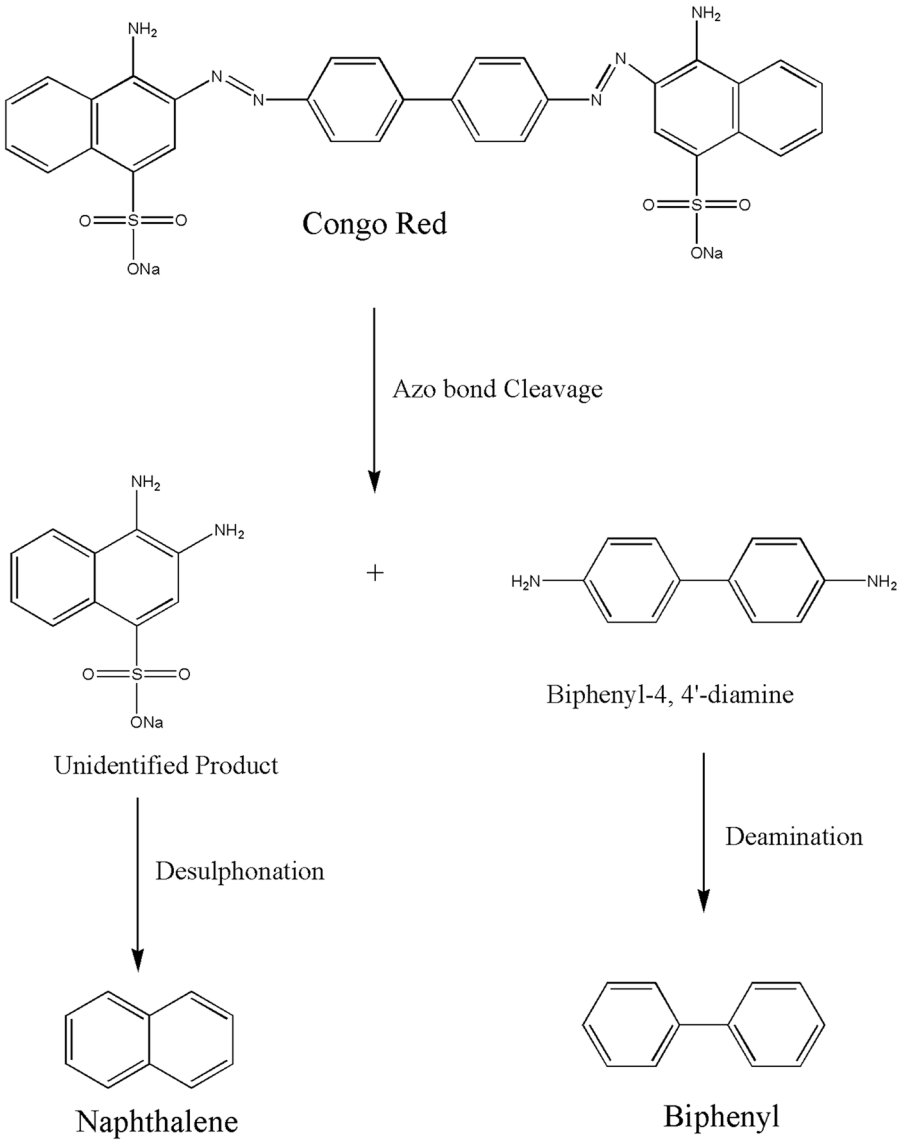

Fig. 10 Degradation pathway of Congo red dye using biosynthesised ZnO-NPs as photocatalyst

The intermediate undergoes deamination to form biphenyl (m/z: 156, molecular weight: 154) as the end product and undergoes desulphonation to form naphthalene (m/z: 129, molecular weight: 128) as by-product [66].

3.7 Mechanism of Photocatalytic Degradation of Congo Red Dye

The possible mechanism of Congo red dye is given in Eqs. (3)-(6). Figure 11 illustrates the degradation of Congo red under UV light. When ZnO nanoparticles are irradiated by a light energy equal to the band gap of energy, the excited electrons move to the conduction band (CB) and create a hole in the valance band (VB) as given in Eq. (3). The atmospheric oxygen reacts with the electron from the conduction band and leads to generation of superoxide radical anion as given in Eq. (4), while H_2O or OH^- combines with h^+ in the valence band to form $HO^{\cdot}$. The resulting $^{-\bullet}O_2/HO^{\cdot}$ reacts with Congo red which is responsible for the degradation as reported [67–73]:

$$ZnO + hv \rightarrow ZnO(h^+ + e^-). \quad (3)$$

$$ZnO(e^-) + O_2 \rightarrow^{-\cdot} O_2. \quad (4)$$

$$H_2O + h^+ \rightarrow HO^{\cdot} + H^+. \quad (5)$$

$$\text{Congo red} + HO^{\cdot}/^{-\cdot}O_2 \rightarrow \text{Degradation pdts.} \quad (6)$$

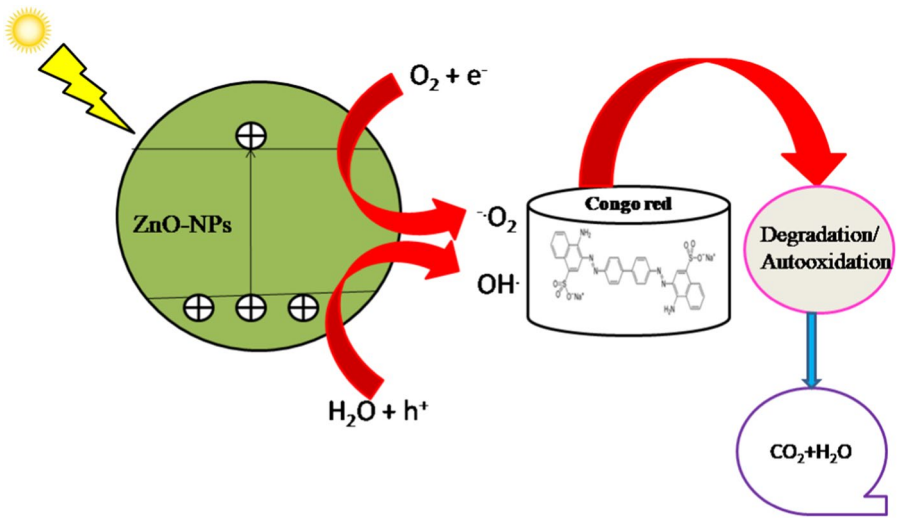

Fig. 11 Photocatalytic degradation mechanism of Congo red

4 Conclusion

A simple and green approach for synthesis of bio-inspired ZnO-NPs using *Ficus hispida* leaf extract as reductant has been reported in this paper. The ZnO-NPs have been characterised by various spectral techniques and found to have wurtzite hexagonal structure with particle size in the range of 20–200 nm. The present study depicts the antitherapeutic activity of biosynthesised ZnO-NPs against DLA cells by trypan blue assay and found to have 96% inhibition at 200 µg mL^{-1}. The anticancer activity of the synthesised ZnO-NPs reveals its potential application as antitherapeutic agent. The photodegradation experiments of Congo red under UV light explore the efficiency of synthesised ZnO-NPs as photocatalysts, and dye is completely removed after 70 min of exposure. The photocatalytic study provides a better alternate for degrading the organic dye contaminants in waste water. The efficiency of the biosynthesiser can be attributed to varying size and agglomeration of biosynthesised ZnO-NPs.

Acknowledgements The authors would like to thank the management of Karpagam Academy of Higher Education and SNS College of Technology for their continous support and facilities provided in the conduction of research.

References

[1] G. Singhal, B. Riju, R.S. Ashish, P.S. Rajendran, Adv. Sci. Eng. Med. **4**, 62 (2012)
[2] A. Van Dijken, E.A. Meulenkamp, D. Vanmaekelbergh, A. Meijerink, J. Lumin. **87**, 454 (2000)
[3] E. Hood, Environ. Health Perspect. **112**, A740 (2004)
[4] M. Ramzaparra, F.Z. Haque, J. Mater. Res. Technol. **3**, 363 (2014)
[5] S. Kalusniak, S. Sadofev, J. Puls, F. Henneberger, Laser Photonics Rev. **3**, 233 (2009)
[6] Y. Li, J. Zhang, Laser Photonics Rev. **4**, 517 (2010)
[7] R.M. Tripathi, A. Saxena, N. Gupta, H. Kapoor, R.P. Singh, Dig. J. Nanomater. Biostruct. **5**, 323 (2010)
[8] R. Patakfalvi, I. Dekany, Colloid Polym. Sci. **280**, 461 (2010)
[9] L. Rodriguez-Sanchez, M.C. Blanco, M.A. Lopez-Quintela, J. Phys. Chem. B **104**, 9683 (2000)
[10] P.B. Taunk, R. Das, D.P. Bisen, R.K. Tamrakar, Optik **127**, 4854 (2016)
[11] R. Sivaraj, P.K. Rahman, P. Rajiv, H. Abdul Salam, R. Venckatesh, Spectrochim. Acta, Part A **133**, 178 (2014).
[12] M. Nasrollahzadeh, M. Sajjadi, J. Dwadashi, H. Ghafuri, Adv. Colloid Interface Sci. **276**, 102103 (2020)
[13] M. Nasrollahzadeh, S. Mahmoudi-Gom Yek, N. Motahharifar, M.G. Gorab, Chem. Rec. **19**, 2436 (2019).
[14] M. Nasrollahzadeh, F. Ghorbannezhad, Z. Issaabadi, S.M. Sajadi, Chem. Rec. **19**, 601 (2019)
[15] M. Bordbar, N. Negahdar, M. Nasrollahzadeh, Sep. Purif. Technol. **191**, 295 (2018)
[16] S.S. Momeni, M. Nasrollahzadeh, A. Rustaiyana, J. Colloid Interface Sci. **472**, 173 (2016)
[17] M. Nasrollahzadeh, S.M. Sajadi, A. Rostami-Vartooni, J. Colloid Interface Sci. **459**, 183 (2015)
[18] K. Kanagamani, P. Muthukrishnan, M. Ilayaraja, K. Shankar, A. Kathiresan, J. Inorg. Organomet. Polym. Mater. **28**, 702 (2018)
[19] M. Murali, C. Mahendra, Nagabhushan, N. Rajashekar, M.S. Sudarshana, K.A. Raveesha, K.N. Amruthesh, Spectrochim. Acta, Part A **179**, 104 (2017).
[20] A. Alkaladi, A. Mohamed Abdelazim, M. Afifi, Int. J. Mol. Sci. **15**, 2015 (2014).
[21] P.A. Arciniegas-Grijalba, M.C. Patiño-Portela, J.P. Mosquera-Sánchez, A. Guerrero-Vargasj, E. Rodríguez-Páez, Appl. Nanosci. **7**, 225 (2017)
[22] S.S. Mydeen, R. Raj Kumar, M. Kottaisamy, V.S. Vasantha, J. Saudi Chem. Soc. **24**, 393 (2020).
[23] M. Nasrollahzadeh, S.M. Sajadi, RSC Adv. **5**, 46240 (2015).
[24] B. Khodadadi, M. Bordbar, M. Nasrollahzadeh, J. Colloid Interface Sci. **493**, 85 (2017)
[25] B. Bhuyan, B. Paul, D. Dhar Purkayastha, S. Sankar Dhar, S. Behera, Mater. Lett. **168**, 158 (2016).

[26] A. Sirelkhatim, S. Mahmud, A. Seeni, N.H.M. Kaus, L. Chuo Ann, S. Khadijah, M. Bakhori, H. Hasan, D. Mohamad, Nano-Micro Lett. **7**, 219 (2015)
[27] A. Hatamifard, M. Nasrollahzadeh, J. Lipkowski, RSC Adv. **5**, 91372 (2015).
[28] M. Maryami, M. Nasrollahzadeh, E. Mehdipour, S.M. Sajadi, Int. J. Hydrogen Energy **41**, 21236 (2016)
[29] S.M. Sajadi, M. Nasrollahzadeh, M. Maham, J. Colloid Interface Sci. **469**, 93 (2016)
[30] F. Ijaz, S. Sammia, S.A. Khan, W. Ahmad, S. Zaman, Trop. J. Pharm. Res. **16**, 743 (2017)
[31] S.A. Khan, F. Noreen, S. Kanwal, A. Iqbal, G. Hussain, Mater. Sci, Eng. C **82**, 46 (2017)
[32] S.A. Khan, F. Noreen, S. Kanwal, G. Hussain, Dig. J. Nanomater. Biostruct. **12**, 877 (2017)
[33] S.A. Khan, S. Shahid, M.R. Sajid, F. Noreen, S. Kanwal, Int. J. Adv. Res. **5**, 925 (2017)
[34] S.A. Khan, S. Kanwal, K. Rizwan, S. Shahid, Microb. Pathog. **125C**, 366 (2018)
[35] S.A. Khan, S. Shahid, S. Kanwal, K. Rizwan, T. Mahmood, K. Ayub, J. Mol. Struct. **1175C**, 73 (1175C)
[36] S.A. Khan, S. Shahid, S. Jabin, S. Zaman, M.N. Sarwar, Dig. J. Nanomater. Biostruct. **13**, 285 (2018)
[37] S.A. Khan, S. Shahid, W. Bashir, S. Kanwal, A. Iqbal, Trop. J. Pharm. Res. **16**, 2331 (2017)
[38] S.A. Khan, S. Shahid, S. Kanwal, G. Hussain, Dyes Pigm. **148C**, 31 (2017)
[39] M.A. Qamar, S. Shahid, S.A. Khan, S. Zaman, M.N. Sarwar, Dig. J. Nanomater. Biostruct. **12**, 1127 (2017)
[40] K. Prakash, P. Senthilkumar, S. Pandiaraj, K. Saravanakumar, S. Karuthapandian, J. Exp. Nanosci. **11**, 1138 (2016)
[41] Z. Belala, M. Jeguirim, M. Belhachemi, F. Addoun, G. Trouve, Desalination **271**, 80 (2011)
[42] N.K. Amin, J. Hazard Mater. **165**, 52 (2009)
[43] H.R. Pouretedal, S. Sabzevari, Desalin. Water Treat. **28**, 247 (2014)
[44] N. Tripathy, R. Ahmad, H. Kuk, J. Photochem. Photobiol. B **161**, 312 (2016)
[45] M. Stan, A. Popa, D. Toloman, A. Dehelean, I. Lung, G. Katona, Mater. Sci. Semicond. Process. **39**, 23 (2015)
[46] M. Nagarajan, K. Arumugam, J. Nanobiotechnol. **11**, 39 (2013)
[47] A.A. Oladiran, I.A. Olabisi, Asian J. Nat. Appl. Sci. **2**, 41 (2013)
[48] H.R. Nawaz, B.A. Solangi, B. Zehra, U. Nadee, J. Sci. Ind. Res. **2**, 164 (2011)
[49] M. Sundrarajan, S. Ambika, K. Bharathi, Adv. Powder Technol. **26**, 1294 (2015)
[50] P.C. Nagajyothi, S. Ju Cha, I. Jun Yang, T.V.M. Sreekanth, K.J. Kim, H.M. Shin, J. Photochem. Photobiol. B **146,** 10 (2015).
[51] M. Stan, A. Popa, D. Toloman, T.D. Silipas, D.C. Vodnar, Acta Metall. Sin.-Engl. Lett. **29**, 228 (2016)
[52] R. Meraat, A.A. Ziabari, K. Issazadeh, N. Shadan, K.M. Jalali, Acta Metall. Sin.-Engl. Lett. **29**, 601 (2016)
[53] S. Azizi, M.B. Ahmad, F. Namvar, R. Mohamad, Mater. Lett. **116**, 275 (2014)
[54] G. Bisht, S. Rayamajhi, Nanobiomedicine **3**, 1 (2016)
[55] P.C. Nagajyothi, T.V.M. Sreekanth, C.O. Tettey, Y.I. Jun, S.H. Mook, Bioorganic Med. Chem. Lett. **24**, 4298 (2014)
[56] J. Suresh, G. Pradheesh, V. Alexramani, M. Sundrarajan, S.I. Hong, Adv. Nat. Sci. Nanosci. Nanotechnol. **9**, 1 (2018)
[57] R.K. Raajshree, D. Brindha, J. Environ. Pathol. Toxicol. Oncol. **37**, 103 (2018)
[58] M. Vishnu Kiran, S. Murugesan, World J. Pharm. Sci. **2**, 926 (2014).
[59] C. Vidya, C. Manjunatha, M.N. Megha Rajshekar, M.A.L. Antony Raj, J. Environ. Chem. Eng. **5**, 3172 (2017).
[60] J. Fowsiya, G. Madhumitha, N.A. Al-Dhabi, M. Valan Arasu, J. Photochem. Photobiol. B **162**, 395 (2016).
[61] E.J. Rupa, L. Kaliraj, S. Abid, D.C. Yang, S.K. Jung, Nanomaterials **9**, 1692 (2019)
[62] S. Chakraborty, J.J. Farida, R. Simon, S. Kasthuri, N. L.M. Averrhoe, Surf. Interfaces **19**, 100488 (2020)
[63] K. Murugesan, K. Tareke, M. Gezehegn, M. Kebede, A. Yazi, G. Diyana, J. Inorg. Organomet. Polym. Mater. **29**, 1368 (2019)
[64] M. Abdus Subhan, M.R. Awal, T. Ahamed, M. Younus, Acta Metall. Sin. -Engl. Lett. **27,** 223 (2014)
[65] K. Nithyadevi, K. Ravichandran, Acta Metall. Sin. -Engl. Lett. **30**, 1249 (2017)
[66] I.S. Ng, T. Chen, R. Lin, X. Zhang, C. Ni, D. Sun, Appl. Microbiol. Biotechnol. **98**, 2297 (2014)
[67] M. Malligavathy, S. Iyyapushpam, S.T. Nishanthi, D. Pathinettam Padiyan, J. Exp. Nanosci. **11**, 1074 (2016).
[68] H. Narayan, H. Alemu, J. Phys.: Conf. Ser. **829**, 1 (2017)
[69] M. Nasrollahzadeh, M. Bagherzadeh, H. Karimi, J. Colloid Interface Sci. **465**, 271 (2016)
[70] Z. Issaabadi, M. Nasrollahzade, S.M. Sajadi, J. Cleaner Prod. **142**, 3584 (2017)
[71] A. Hatamifard, M. Nasrollahzadeh, S.M. Sajadib, New J. Chem. **40**, 2501 (2016)
[72] M. Nasrollahzadeh, Z. Issaabadia, S.M. Sajadib, Compos. B **166**, 112 (2019)
[73] M. Nasrollahzadeh, Z. Issaabadia, H.R. Dasmeh, H.M. Sajadi, J. Alloys Compd. **763**, 1024 (2018)